Growth and Oxygen Stoichiometry Control of High-Quality La 2 CoO 4+δ Single Crystals (δ = 0.25)

Ruben de Barros, Monica Ceretti, Wolfgang Schmidt, Vladimir Pomjakushin, Werner Paulus

Growth and oxygen stoichiometry control of high quality $La_2CoO_{4+\delta}$ single crystals ($\delta = 0.25$)

Ruben De Barros [a], Monica Ceretti [a], Wolfgang Schmidt [b], Vladimir Y. Pomjakushin [c], Werner Paulus [a]*

a ICGM, Univ Montpellier, CNRS, ENSCM, 34000 Montpellier, France

b Forschungszentrum Jülich GmbH, Jülich Centre for Neutron Science at ILL, 38042 Grenoble, France

c Laboratory for Neutron Scattering and Imaging, Paul Scherrer Institut (PSI), CH-5232 Villigen PSI, Switzerland

KEYWORDS. Single crystal growth, floating zone, correlated oxides, $La_2CoO_{4+\delta}$.

ABSTRACT. $La_2CoO_{4+\delta}$ is a strongly correlated oxide with exciting physical and electronic properties originating from the subtle interplay of lattice, orbital, charge, and spin degrees of freedom. In particular, the oxygen rich $La_2CoO_{4.25}$ is a key compound for studying oxygen and electronic ordering phenomena and their correlation. Single crystal growth of these phases has been plagued by difficulties related to its incongruent melting. In this work, we report on the

growth and characterization of high quality, centimeter sized $La_2CoO_{4.25}$ single crystals, suitable for neutron scattering experiments. $La_2CoO_{4+\delta}$ single crystals were grown by the Travelling Solvent Floating Zone (TSFZ) without the addition of a solvent but continuously stabilizing the growth conditions. Post synthesis annealing at 500°C in oxygen flux yielded phase pure $La_2CoO_{4.25}$, which was further characterized by single crystal neutron and X-ray diffraction, as well as by electron microscopy (SEM/EDS), revealing its quality in terms of composition, homogeneity and crystalline quality. For $La_2CoO_{4.25}$ a complex structure with a 2D modulation vector related to oxygen ordering was revealed by single crystal X-ray and neutron powder diffraction studies. In addition, magnetic measurements coupled with preliminary single crystal elastic neutron scattering experiments exhibit antiferromagnetic ordering with a Néel temperature of $T_N = 36$ K with a complex magnetic structure involving a doubling of all orthorhombic axes.

Introduction

Transition metal oxides with layered perovskite frameworks have been extensively studied, due to their interesting electronic properties.[1-4] Among them, Ruddlesden-Popper (RP) oxides with a general formula A_2BO_4 are strongly correlated electronic systems with exciting physical and electronic properties originating from the subtle interplay of lattice, orbital, charge, and spin degrees of freedom. They also show a very good oxygen ion conductivity at moderate temperatures, promoting them to be among the most promising candidates for oxygen membranes or electrodes in solid oxide fuel cells (SOFCs) as well as Solid Oxide Electrolysis Cell (SOEC) devices.[5-7] Their structure consists of an alternating stacking of A_2O_2 rock-salt and infinite BO_2 layers along the *c*-axis, as schematically shown in Figure 1. The ionic conductivity mechanism of these materials has been associated with the excess

interstitial oxygen (δ) accommodated inside the rock-salt layers, inducing strongly anharmonic displacements of all apical oxygen, thus creating a shallow 1D oxygen diffusion pathway between apical and interstitial oxygen sites.[8, 9] In this context, room temperature oxygen diffusion has been reported recently during a topotactic oxygen release reaction in $Pr_2NiO_{4.25}$, together with the co-existence of sub-mesoscopic oxygen ordering involving translational periodicities of more than 100 Å.[10]

Co-based RP phases $La_2CoO_{4+\delta}$, with $0 \leq \delta \leq 0.25$, are attractive as they are still today the only non-stoichiometric transition metal oxide for which spontaneous oxygen uptake at ambient conditions was reported, yielding unusually high diffusion coefficients combined with unexpectedly low activation energies.[11, 12]

In addition, $La_2CoO_{4+\delta}$ is particularly relevant in terms of electronic correlations, providing a unique opportunity to study interplay between dimensionality, lattice, charge spin and orbital momentum degrees of freedom. The Co valence state can be tuned by substituting the La^{3+} rare-earth atoms by 2-foldly charged alkaline earth metals A^{2+} (hole doping), or simply by oxygen doping, forming $La_{2-x}A_xCoO_4$ or $La_2CoO_{4+\delta}$ respectively. With a typical range of $0 \leq \delta \leq 0.25$, the formal valence of the Co cations partially ranges from (II) to (III). The remarkable difference is that cation substitution requires high synthesis temperatures, resulting into an average distribution of the A-cations, while oxygen is still mobile even at RT, allowing to form long-range ordering of the interstitial oxygen atoms.[10, 13] Lattice, i.e. long-range oxygen ordering, is consequently added as a fourth degree of freedom to the charge, spin and orbital ordering.[14]

Oxygen insertion and related structural and electronic ordering have been much less investigated compared to A-cation type compounds.[15-19] This is essentially related to the fact that adjusting defined oxygen stoichiometries i.e. achieving phase homogeneity is a difficult

task. Moreover, oxygen doped phases have often been reported to show ordering schemes, which were not always reproducible.

At room temperature, stoichiometric $La_2CoO_{4.00}$ shows the LTO (Low Temperature Orthorhombic) octahedral tilting arrangement (space group *Bmab*). Small quantities of intercalated oxygen are, however, sufficient to induce local structural distortions as the extra oxygen atoms are located on interstitial lattice sites. This involves the disappearance of the superstructure reflections related to the 3D ordering of the CoO_6 octahedra, reducing the space group symmetry to *Fmmm* (Figure 1). Further intercalation of oxygen leads for higher doping concentrations to the formation of complex superstructures, related to oxygen ordering.[13]

Among the oxygen doped phases, $La_2CoO_{4.25}$ showing the highest achievable oxygen stoichiometry is particularly interesting. Containing an equal amount of Co^{2+}/Co^{3+}, it is the analogous to half-hole doped $La_{1.5}Sr_{0.5}CoO_4$, showing a loosely correlated checkerboard charge ordering of Co^{3+} and Co^{2+} ions.[16, 18-21] To this, long-range oxygen ordering may go along with complex electronic ordering, as observed for the spin structure in the homologous $Nd_2NiO_{4.10}$[10], yielding to interesting correlations.[14, 22]

Ordering phenomena and their interplay are generally difficult to explore related to weak satellite intensities and the availability of single phases. The availability of high purity single crystals, suitable for elastic and inelastic neutron scattering studies, are thus mandatory.

Therefore, we investigated the growth of large and high quality $La_2CoO_{4.25}$ single crystals, intended to perform future investigations by synchrotron/neutron diffraction as well magnetic excitations by inelastic neutron scattering.

Among the different single-crystal growth techniques, the travelling floating zone method shows several advantages, as the absence of impurities compared to methods using crucibles, and thus the possibility to obtain high quality single crystals of sufficiently large size for

accurate structural and dynamics characterisation. Growing high-quality $La_2CoO_{4+\delta}$ single crystals is however particularly difficult due to the incongruent melting behaviour and only few works have been reported so far.[13, 23-26]

In the present work, we report on $La_2CoO_{4+\delta}$ (with $\delta = 0.25$) crystal growth conditions to obtain centimetre sized, high quality single crystals by the floating zone method, and their characterization by scattering techniques (neutron and X-ray diffraction). Magnetic behaviour is also explored by magnetization measurements as well as preliminary elastic neutron scattering experiments.

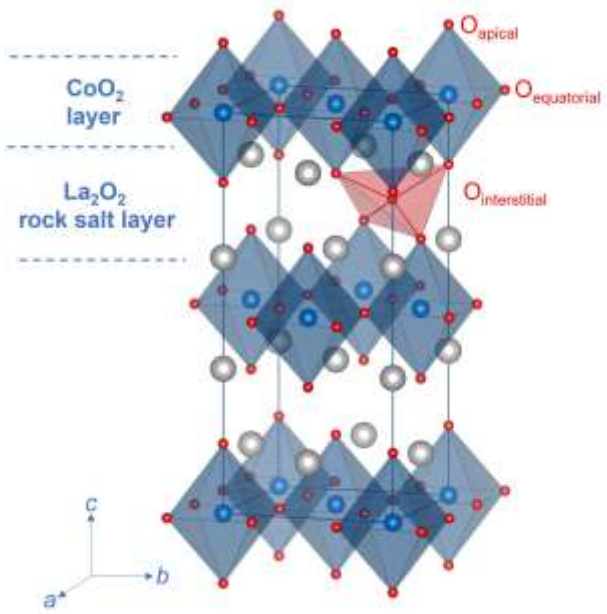

Figure 1: *F*-centred crystallographic structure of orthorhombic $La_2CoO_{4.25}$ (blue: Co, red: O, grey: La). Interstitial oxygen atoms are located in the La_2O_2 rock salt layer, tetrahedrally coordinated by the apical oxygen as well as La atoms. Here only one out of 8 possible equivalent O_{int} positions is shown, the average occupation being 1/8.

Experimental section

Synthesis and single crystal growth. $La_2CoO_{4+\delta}$ starting material for feed and seed rods was prepared by classical solid-state reactions at high temperature, beginning from the precursor binary La_2O_3 and Co_3O_4 oxides. Prior to the synthesis, La_2O_3 was heated in dynamic primary vacuum at 900°C overnight to remove any hydroxide traces. Stoichiometric amounts of La_2O_3 and Co_3O_4 powders (99.99% purity, Alfa Aesar) were then thoroughly ground, and calcinated for 12h at 900 °C in air. The obtained powders were then grinded again, pressed in pellets and sintered at 1250°C for 24 h in argon flux to avoid the formation of $LaCoO_3$. This step was repeated two times with intermediate grinding and pelletizing. Seed and feed rods for crystal growth were obtained by hydrostatic pressing of the as synthesized $La_2CoO_{4+\delta}$ powders at 10 bars in a cylindrical latex tube of 6 mm in diameter and 120 mm in length. A subsequent sintering at 1250°C for 18 h in argon allowed obtaining very dense polycrystalline rods for single crystal growth. The crystal growth was carried out by the travelling floating zone (TFZ) method, using a two-mirror optical floating zone furnace (NEC SC2, Japan) equipped with two 500 W halogen lamps. Their low-sized filaments allowed steepening the temperature gradient around the molten zone to maintain the stoichiometry of the feed rod as stable as possible before it enters the molten part.

The growth was carried out in argon flux (Ar 99,999%) with a speed rate of 1 mm/h and the feed and seed rods counter rotating at 10 rpm. After growing, the crystal has been annealed in flowing oxygen at 500 °C for 12 hours with a cooling ramp of 0.2 °C/ min down to room temperature.

X-ray and neutron diffraction. Phase purity of the grown crystals were checked by laboratory X-ray powder diffraction on a Bruker D8 Discover diffractometer equipped with a Johansson monochromator for $CuK\alpha_1$ radiation and a fast detector with high energy resolution

(LynxEye XE-T). Powder diffraction patterns were analyzed using the FullProf suite[27] and the crystal structure is visualized using the VESTA freeware.[28] The orientation of the as grown single crystals was investigated by X-ray Laue diffraction in backscattering mode, using a tungsten anode on a Seifert generator, equipped with an image plate detector (Fuji). Data were analyzed using the Orient Express V3.3 software. Further on, the bulk crystal quality of a centimeter sized crystal was checked using the two-axis neutron test diffractometer ORION[29] (λ=1.73 Å) of the Swiss Spallation Neutron Source (SINQ) at the Paul Scherrer Institute. Complementary neutron powder diffraction (NPD) measurements on a crushed single crystal were performed on the high-resolution diffractometer HRPT (λ = 1.49 Å) at the PSI, with the aim to precisely determine the oxygen content of the compound. Additional neutron scattering measurements were performed on the cold neutron three-axis spectrometer IN12 at the Institut Laue Langevin (Grenoble) to follow the antiferromagnetic ordering. IN12 has been used in its standard configuration, with focusing graphite monochromator and analyser. As sample environment a standard ILL orange cryostat was used.

Single crystal X-ray diffraction (SXRD) studies were carried out using a STOE-STADIVARI (MoK_α source, Xenocs Microfocus tube) diffractometer equipped with a Dectris 200K Pilatus pixel-detector. A needle shaped single crystal with 0.1mm diameter was glued on a glass capillary and used for X-ray diffraction studies. Intensity data were collected with psi-scan mode at different chi positions for reciprocal space scanning.

Electron microscopy. The crystal elemental composition was checked by Scanning Electron Microscopy (SEM) analysis using a FEI Quanta 200 FEG microscope equipped with an Energy Selecting X-ray microanalysis (EDS) system with an Oxford Instruments Ultim Max 100 mm^2 Silicon Drift Detector (SDD) for atomic recognition via X-ray fluorescence spectroscopy. SEM/EDS analyses have been performed on a cross section (4 mm in diameter) of the grown crystals, after an accurate surface polishing and cleaning.

Magnetic measurements. Magnetization measurements were performed with a superconducting quantum interference device (SQUID) magnetometer MPMS 7XL (Quantum Design magnetic property measurement system) on a small crystal, fixed in a gelatin capsule and then inserted in a plastic straw. Measurements were made by the dc method with a constant applied magnetic field of 500 Oe from 2 to 300 K.

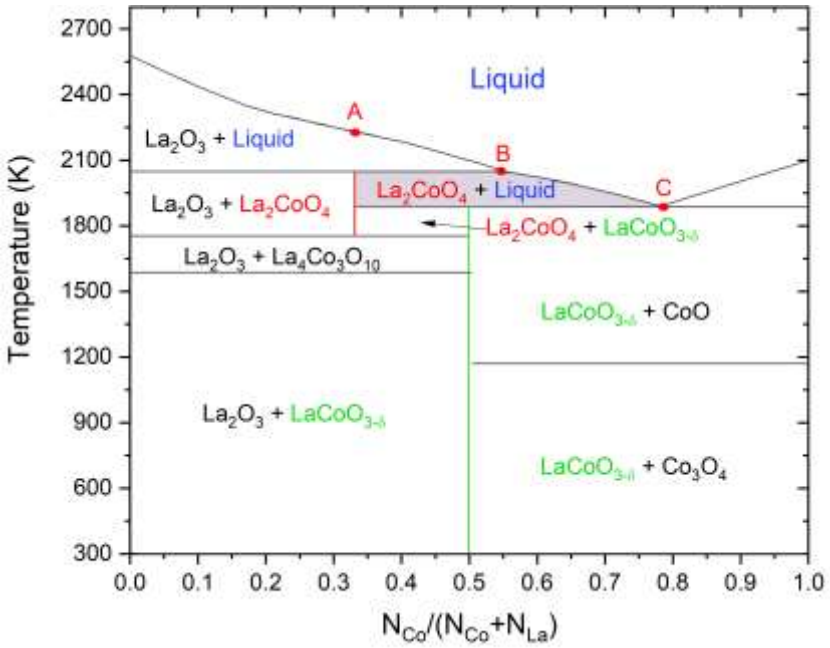

Figure 2. Phase diagram of La-Co-O system as a function of the temperature, adapted from ref [30]

Results and Discussion

Crystal Growth.

According to the reported La/Co/O phase diagram (Figure 2), La_2CoO_4 melts incongruently at around 2050 K with an eutectic temperature of 1885K.[30] Therefore, LCO single crystals can only be grown within this narrow temperature range, using a melt with a Co:La molar

ratio approximately between 1.22:1 and 4:1, corresponding to the B-C line in the phase diagram in Figure 2). Generally, the few works reported in the literature on the growth of La_2CoO_4 single crystals have been carried out by the Travelling Solvent zone method, using an increased Co concentration for the travelling solvent.[13, 25] In the present work, we applied a different approach: instead of preparing a pre-enriched CoO solvent flux rod separately, a suitable molten zone has been achieved by using the same stoichiometric feed and seed rod already from the beginning of the growth, but which gets self-adjusted with the solidification of La_2O_3, thereby continuously enriching the Co-amount in the traveling solvent. To adjust the molten zone stoichiometry from the initial incongruently melted stoichiometric feed rod and to stabilize the required La:Co molar range close to 1.22:1 and 4:1, the zone is first heated to T above 2240K (point A in Figure 2), reaching the liquid phase. Upon slowly cooling, the zone enters a two-phase region consisting of solid La_2O_3 and liquid. As the zone starts to travel, La_2O_3 crystallizes at the trailing edge supplying extra Co to the melt and thus lowering the melting temperature. Stable growth condition are achieved when the molten zone reaches the Co:La molar ratio in the range discussed above, before reaching the eutectic point. Thus, through the initial heating and cooling process with constant pulling simultaneously, it was possible to obtain a self-adjusted molten zone with the required La:Co ratio. Although all the precautions taken, the growth process remains very delicate as it is constantly perturbed by small fluctuations of the growth conditions requiring a continuous adjustment of the lamp power. Nevertheless, once a steady molten zone is achieved, stable growth conditions could be maintained almost for the whole process i.e. 2-3 days; the optimum growth conditions were achieved at 1mm h^{-1} growth velocity and 10 rpm counter rotating. Figure 3a shows a representative as-grown $La_2CoO_{4+\delta}$ single crystal with a diameter of 4 mm and a length of 50 mm, with a shiny, silver-black surface of metallic lustre. The initial region of about 5 mm in length contained a mixture of La_2O_3 and La_2CoO_4. Thus, when

the crystal was left in air for a few days, this initial region disintegrates and became a white powder, identified as $La(OH)_3$ by powder XRD. Despite this, the as grown crystal was sufficiently in size, allowing to extract a homogeneous, 4 cm long piece, suitable for neutron scattering measurements.

A shiny facet is present along the whole length of the as grown crystal (Figure 3a). Laue diffraction has identified this plane to correspond to (001), i.e. the *c* axis being perpendicular to the crystal axis, while the growth direction (crystal axis) is [210], with respect to the *Fmmm* unit cell (Figure 3c).

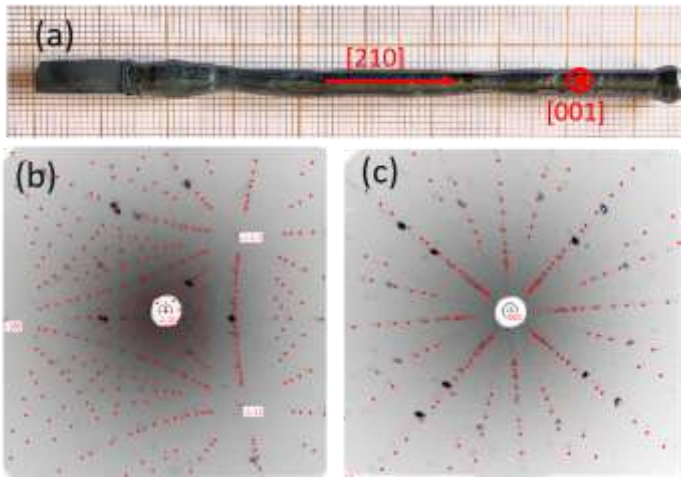

Figure 3. (a) A representative as-grown $La_2CoO_{4+\delta}$ single crystal obtained by the TFZ method in Ar atmosphere. (b-c) X-ray Laue patterns obtained under backscattering conditions: (b) taken perpendicular to crystal axis, showing the (210) growth direction and (c) for one of the facets of the crystal, which turned out to be the *c* axis.

Chemical composition and homogeneity of the crystals were checked by SEM coupled with EDX analysis. For this purpose, a slice of the crystal was taken perpendicular to the growth direction and polished mechanically. The crystals were found to be free of cracks or inclusions of secondary phases (Figure 4b-c). Different points throughout the cross-section of the crystal

were analysed to verify the chemical composition as well as its homogeneity. It was found that the atomic percentage of La and Co, are constant over the whole cross section, the La/Co ratio being 2.09 ± 0.05, which corresponds to the Co content of 0.96 ± 0.05 (Figure 4a). A slight Co under-stoichiometry has also been found in previous works, probably due to the volatility of CoO during high temperature synthesis. However, we did not observe any significant evaporation of the material during crystal growth.[25]

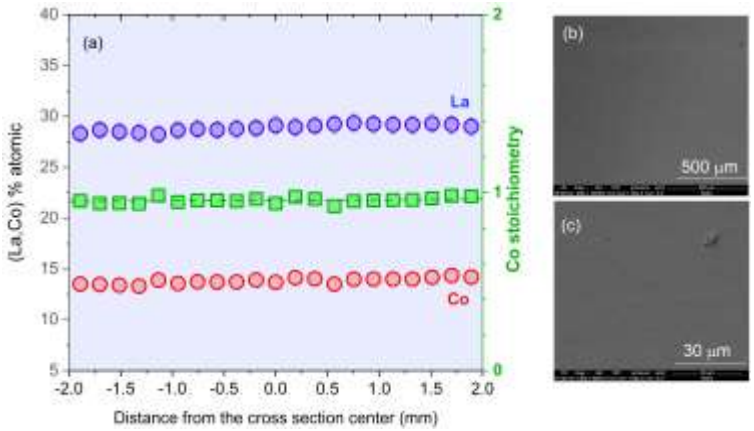

Figure 4. (a) Atomic distribution (% at.) of La (blue circles) and Co (red circles) over a cross section of the as-grown $La_2CoO_{4+\delta}$ crystal with a diameter of 4 mm. The respective Co stoichiometry is indicated as green squares. (b-c) SEM images (at different scales) of portions of the crystal cross section, showing the absence of cracks or intergrowth phases.

To check the phase purity, powder X-ray diffraction has been carried out on crushed parts of the as grown crystal, taken at different positions along the crystal. From the corresponding XRD patterns, as shown in Figure 5, the as grown $La_2CoO_{4+\delta}$ does not present any impurities, but different phases with distinct oxygen content were identified. Figure 5a shows the existence of an orthorhombic phase (SG: *Fmmm)* together with a tetragonal one (*F4/mmm*), as revealed by profile matching using the Fullprof software suite. Refined lattice parameters for the orthorhombic and tetragonal phase are: a= 5.4751(1) Å, b = 5.5319(1) Å and c = 12.6363(3)

Å) as well as $a = b = 5.5006(1)$ Å and $c = 12.6166(5)$Å. We could also uncover a phase showing a symmetry reduction towards monoclinic as outlined in Figure 5b, as becomes evident from the splitting of the (220/-220) reflection, and which subsequently was refined in the space group *F112/m*, with $a = 5.4783(1)$ Å, $b = 5.5299(2)$ Å, $c = 12.6126(2)$ Å, and $\gamma = 90.076(5)°$.

The existence of a monoclinic symmetry has never been reported for LCO, while it is common for oxygen doped Ruddlesden-Popper phases as $(Pr/Nd)_2NiO_{4.25}$,[14, 31] and it is presently under investigation.

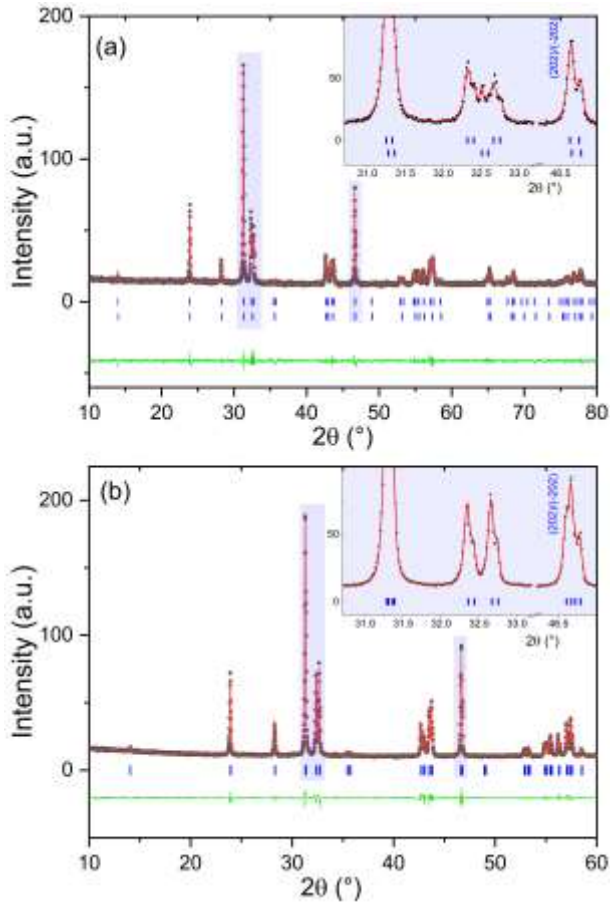

Figure 5. X ray diffraction patterns of crushed $La_2CoO_{4+\delta}$ crystal, obtained at two different position of the as grown crystal. (a) Mixture of the orthorhombic *Fmmm* and tetragonal *F4/mmm* phases and (b) monoclinic *F112/m* phase, showing the (220) monoclinic splitting (in the inset).

In order to adjust a homogeneous oxygen content over the entire crystal, post-synthesis annealing of the crystal under defined conditions has been carried out. The crystal was hold for 12h at 500 °C in pure O_2 atmosphere, following a controlled cooling with a rate of 0.2°C/min to ambient. To verify the phase purity, the as obtained single crystals were crushed and analyzed by Rietveld refinement on X-ray diffraction data, yielding a single phase with orthorhombic symmetry (SG: *Fmmm*) and lattice parameters a = 5.4804(1), b = 5.5326(1) and c = 12.5397(2) (Figure 6). These lattice constants correspond to the oxygen rich phase $La_2CoO_{4.25}$ ($\delta = 0.25$)[12].

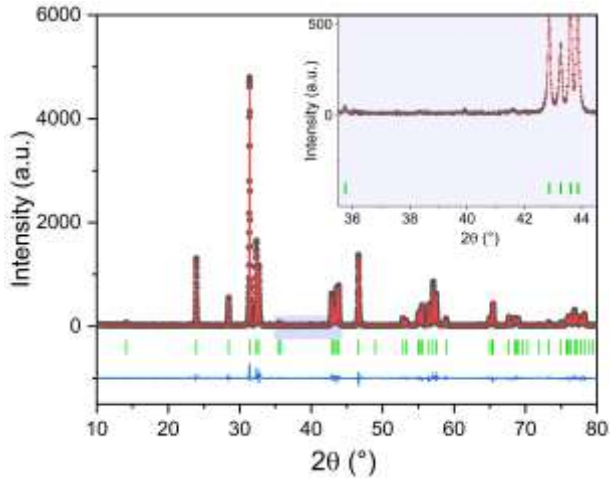

Figure 6. X-ray diffraction pattern of the crushed single crystal at RT, after annealing in pure oxygen flow at 500°C, showing the oxygen rich phase $La_2CoO_{4.25}$ with *Fmmm* symmetry. Data have been collected on the Brucker D8 Discover X-ray diffractometer with $CuK_{\alpha 1}$. Black dots are the experimental data while the calculated patterns are represented by continuous red lines. The lowermost blue continuous line represents the difference between the experimental and calculated intensities and the short green vertical bars mark the structural Bragg peaks and of the satellite reflections.

Single crystal X-ray diffraction

The oxygen annealed $La_2CoO_{4.25}$ single crystals were consequently further investigated by X-ray single crystal diffraction. Figures 7a and 7b show the reconstructed (*hk4*) and (*hk0*) layers obtained on the single crystal STOE STADIVARI diffractometer. The lattice metric is compatible with the *mmm* Laue class and *Fmmm* space group. In addition, the basic reflections show the typical splitting, related to the orthorhombic twining, as a consequence of the symmetry reduction related to the HTT to LTO phase transition during the single growth, involving two orthorhombic twin domains sharing a common $(\bar{1}10)$-plane. On top of the main reflections, a huge number of satellites become visible. At first sight all additional superstructure reflections can be indexed on the basis of a $4\boldsymbol{a} \times 4\boldsymbol{b} \times 4\boldsymbol{c}$ supercell. However, the systematic absence of a vast majority of allowed reflections within this supercell renders such a formal indexation questionable. An alternative description can be obtained using a formalism, which has been applied successfully to the oxygen ordered homologous phase $Pr_2NiO_{4+\delta}$. This implies the formation of a 3D modulated structure with commensurate modulation vectors. It assumes a modulation vectors $\mathbf{q}_n = \alpha\mathbf{a}^*+\beta\mathbf{b}^*+\gamma\mathbf{c}^*$ added to the position of each Bragg reflection $\mathbf{G} = h\mathbf{a}^* + k\mathbf{b}^* + l\mathbf{c}^* + m\mathbf{q}_n$, where m is an integer number representing the order of corresponding superstructure reflections. The modulation vectors were found for $La_2CoO_{4.25}$ to be $\mathbf{q}_n = \pm\, 0.75\mathbf{a}^* + 0.50\boldsymbol{b}^*$, as indicated in Figure 7a for one out of the four domains by a red dotted line. This is equivalent to a commensurate description with a ($6a \times 4b$)-unit cell (Figure 7c).

The patterns can then be indexed assuming two orthorhombic twin domains, with each two modulation vectors, resulting in four independent modulation vectors (for clarity's sake only one vector is indicated in Figure 7a), and considering harmonics of up to fourth-order. The corresponding simulation of the peak positions are indicated by red circles in Figure 7a-b.

Besides these reflections, we also observed *P*-type reflections (cyan circles), indicating a deviation from *F*-centring, making the true lattice translation to be primitive. Further studies are in progress to extract the true symmetry and space group. Interestingly, there are a few additional reflections which cannot be indexed within this formalism, showing half integer values at $h = ½$ or $k = ½$ and which are indicated by green circles (Figure 7a-b). They might be attributed to electronic ordering phenomena, *e.g.* charge ordering of Co^{2+}/Co^{3+}, as they would perfectly correspond to a checkerboard-type charge order as found in hole-doped $La_{1.5}Sr_{0.5}CoO_4$. Further studies to explore the T-dependence of the different types of satellite reflections are presently in progress. We anticipate here the peculiar behaviour that on top of the structural reflections such as (0.5, 1 0), (1, 0.5, 0) or (1.5, 0, 0), magnetic intensities are observed on IN12@ILL, as it will be discussed in the low-T neutron diffraction part below.

While the positions of the satellite reflections can be precisely simulated, their intensities cannot. Since a decrease in the intensity is expected to go along with the order of the satellites, the simulations consider a relative intensity description with the diameter of the circles being largest for the basic reflection, while decreasing for 1st order and finally becoming smallest for the 4th order satellites. Similar incommensurate structure schemes have been reported for nickelates and cobaltates,[10, 13, 32] underlying the more general character of complex structural oxygen ordering in K_2NiF_4-type oxides as a function of δ.

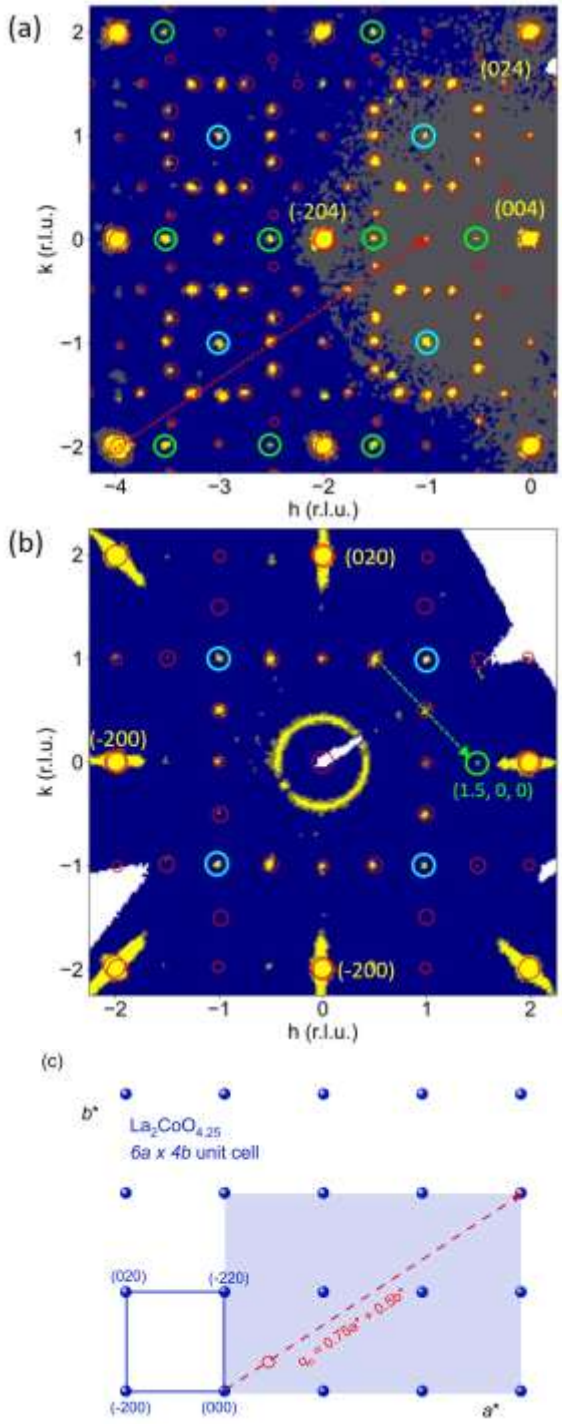

Figure 7. (a-b) Section of reconstructed *(hk4)* and *(hk0)* planes obtained with single X-ray diffraction (STOE STADIVARI, MoK$_\alpha$) measurements on a $La_2CoO_{4.25}$ single crystal, after annealing (500°C) in O_2, and subsequent slow cooling down to room temperature. Simulated positions of the superstructure reflections for the *(hk4)* and *(hk0)* sections are overlaid on the experimental data with red circles. The superstructure reflections correspond to modulation

vectors **q** = ± 0.75**a***+0.5**b*** (the corresponding vector scheme for the indexation of up to the fourth order is indicated by the dotted red line). The simulations consider a relative intensity description with the diameter of the circles being largest for the basic reflection while decreasing with the increasing order of satellites. (c) Translational scheme in the (a*,b*) plane, corresponding to a commensurate unit cell 6*a* × 4*b*.

Single crystal neutron diffraction. The crystalline quality of the oxygen annealed $La_2CoO_{4.25}$ crystals, including possible twinning, was assessed by neutron diffraction on centimetre sized samples on the ORION diffractometer at SINQ (PSI, Switzerland). In addition to being a nondestructive technique, the negligible absorption of neutrons by the samples means that neutron diffraction gives truly bulk information, while the penetration depth of X-rays is limited to several micrometres only. To this end, the crystal was aligned with the *c*-axis perpendicular to the diffraction plane of the diffractometer; pure transversal scans (ω scans) were carried out for characteristic reflections such as (*hh0*) and (*00ℓ*), in order to determine the peak width, and thus related bulk crystalline quality.

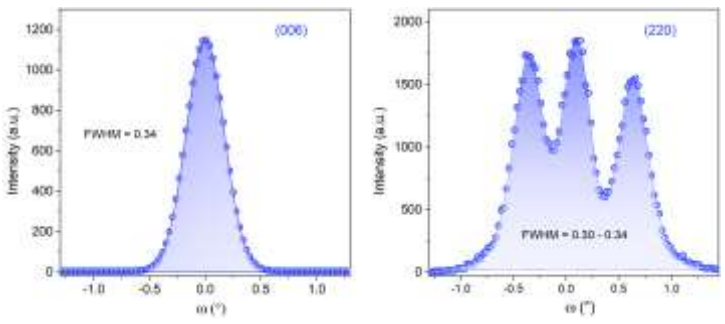

Figure 8. ω-scans of the (006) and (220) reflections of $La_2CoO_{4.25}$ obtained on ORION@PSI (λ=1.73Å) (FWHMs are in degree).

.

As shown in Figure 8, the full width at half maximum (FWHM) for all reflections is about 0.3°, which is within or close to the respective instrumental resolution[29], thus demonstrating the high crystalline quality of the $La_2CoO_{4.25}$ single crystal. The ω-scans for the (*hh0*) reflections, i.e. the (220) and the equivalent (−220) reflections, show three distinct reflections, which agrees well with the formation of totally four twin domains, related to the HTT to LTO phase transition during the single crystal growth.[33]

The sharp profiles of the (220) as well as the (006) reflections also indicate a homogeneous oxygen stoichiometry all over the crystal, as any inhomogeneity of δ is expected to result in significant profile broadening related to changes in the lattice parameters.[12] The high crystalline quality of the crystal was also confirmed on the triple axis spectrometer IN12@ILL (see below), where the elastic diffraction peaks are sharp, perfectly gaussian, without broadening or asymmetries.

Neutron powder diffraction

The total oxygen content as well as the nuclear structure were investigated by neutron powder diffraction on the crushed $La_2CoO_{4.25}$ single crystals. Neutrons are more sensitive towards low-Z elements as oxygen, allowing to reliably determine the amount of the oxygen doping concentration in the structure. The neutron powder diffraction data as well as the refined structural parameters of $La_2CoO_{4.25}$ collected at 50 K on HRPT (PSI, Switzerland) are reported in Figure 9 and in Table 1, respectively. To take into account the large anisotropic displacement factors for the apical oxygen atoms (O_{ap}), a split position for O_{ap} has been applied using (0, 0, z with $z \approx 0.18$) as well as (x, y, z), thereby constraining both z parameters to be identical, while their occupation was constrained to yield the full site occupation 2.

Refinement of the oxygen occupancy on the interstitial sites confirms the oxygen content $\delta = 0.255(5)$; moreover, the refined Co occupancy of 0.976(13) agrees well with the EDX results presented above.

Additional reflections, related to the modulated oxygen ordering presented above for the single crystal X-ray diffraction, are also visible in neutron powder diffraction (inset Figure 8). The modulation vector $\mathbf{q} = 0.75\mathbf{a}^*+0.50\mathbf{b}^*$, as obtained by single crystal diffraction, has been introduced as starting parameter for the refinement of the NPD data. Due to the significant intensity reduction between 1st and 2nd order satellite reflections, the pattern can already be fitted considering only the 1st order satellite reflections, yielding a refined modulation vector $\mathbf{q} = \pm 0.7535(2)\mathbf{a}^* + 0.4985(1)\mathbf{b}^*$. Similar incommensurate structure schemes have been reported for nickelates and cobaltates,[10, 13, 32, 34] underlying the more general character of complex structural oxygen ordering in K_2NiF_4-type oxides as a function of δ. We note that all satellite reflections visible in the NPD pattern can be indexed, assuming the modulation vector related to oxygen ordering only, i.e. no further satellites with *h/2* or *k/2* type indexation, as well as *P*-type indexing is necessary to consider, which underlines the hypothesis that the latter are related to charge ordering. It suggests that the Co^{2+}/Co^{3+} charge ordering as indicated from the single crystal X-ray diffraction data, is already installed at ambient.

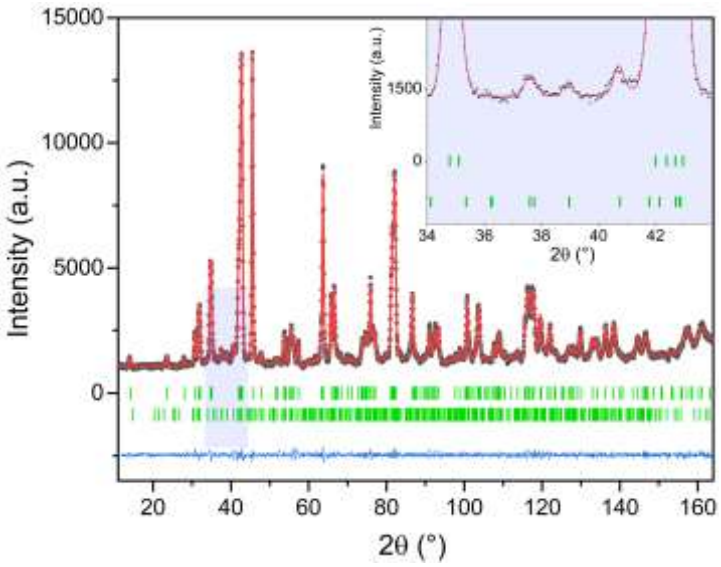

Figure 9. NPD pattern of the $La_2CoO_{4.25}$ crushed crystal showing superstructure reflections due to oxygen ordering, with a refined modulation vector **q** = 0.7535(2)**a*** + 0.4985(1)**b***. The inset is a zoomed view of the shaded blue section highlighting the presence of oxygen superstructure peaks, which are barely observable but impossible to fit in the corresponding XRD pattern (shown in the inset of Figure 6). Black dots are the experimental data while the calculated patterns are represented by continuous red lines. The lowermost blue continuous line represents the difference between the experimental and calculated intensities and the short green vertical bars mark the structural Bragg peaks and of the satellite reflections. Diffraction data have been taken on the high resolution HRPT diffractometer at the PSI (λ=1.494 Å).

Table 1. $La_2CoO_{4.25}$ structural data obtained at 50 K from powder neutron diffraction data, collected on the high resolution HRPT diffractometer at the PSI, with λ=1.49 Å. Refinements were carried out in space group *Fmmm*. [a]

Atom	x	y	z	occ.	U_{iso} (Å^2)	
La	0	0	0.3589(1)	2.00	0.0092 (2)	
Co	0	0	0	0.976(13)	0.0105(10)	
O_{ap1}	0	0	0.1685(13)	1.096(13)	0.0136(13)	
O_{ap2}	0.9379(9)	0.9196(9)	0.1685(13)	0.904(13)	0.0136(13)	
O_{eq}	¼	¼	0	1.969(12)	0.0094(6)	U_{11} = 0.0094(4) U_{22} = 0.0024(5) U_{33} = 0.0166(7) U_{12} =-0.0010(4)
O_{int}	¼	¼	¼	0.255(7)	0.012(2)	

[a]lattice parameters: a = 5.4706(2), b = 5.5289(1) Å, c = 12.5141(3) Å; R_p = 2.78%, R_{wp} = 3.62%, χ^2 = 1.3

Magnetic studies

Field-cooled (FC) and zero-field-cooled (ZFC) magnetization measurements were investigated on $La_2CoO_{4.25}$ (45mg) using a SQUID. The temperature dependence of the FC and ZFC susceptibility χ is shown in Figure 10a. Both curves mostly overlay upon each other in the temperature range 30 – 300 K with a cusp at 36 K, indicating the onset of an antiferromagnetic transition (T_N). Below 30 K, χ_{ZFC}(T) and χ_{FC}(T) bifurcate from each other, suggesting the presence of irreversibilities (magnetic metastability) in the system due to some magnetic frustrations persisting locally above T_N, imposing the magnetic moments to partially remain in a spin glass state.

Although an in-depth characterization of magnetism in $La_2CoO_{4.25}$ is out of the scope of this work, the inverse of the magnetic susceptibility (Figure 10b) in the paramagnetic region (T >

T_N) provides first information about the effective paramagnetic moments (μ_{eff}). Thus, the high temperature region (above 70 K) of $\chi^{-1}$was modeled with the modified Curie–Weiss equation $\chi = \frac{C}{T-\theta_{CW}}$, where *C* the Curie constant and θ_{CW} is the Curie–Weiss temperature. The resulting fit yielded a μ_{eff} = 3.79 μ_B and θ_{CW} = -89 K, which are similar to those reported for $La_{1.5}Sr_{0.5}CoO_4$.[35] The oxygen content in the compound implies a formal valence state attribution corresponding to $La_2(Co^{2+}/Co^{3+})O_{4.25}$, i.e. an equal amount of the cobalt ions corresponding to Co^{2+} and Co^{3+}. From this assumption, the experimental effective moment matches well with a high spin Co^{2+} ion (electronic configuration d^7: $t_{2g}^5e_g^2$, S = 3/2, L = 3) with an unquenched orbital moment that is fully decoupled from the spin contribution, as calculated from $\mu_{L+S} = \sqrt{4S(S+1)+L(L+1)} = 5.20\mu_B$, while Co^{3+} is in the low spin configuration (S=0) and thus non-magnetic. The effective magnetic moment, considering magnetic Co^{2+} together with low-spin Co^{3+}, yields a μ_{eff} = 3.68 μ_B, in good agreement with the experimental results.

As for the Sr doped counterpart, the magnetization on the oxygen doped $La_2CoO_{4.25}$ have to be assigned to Co^{2+} only, while the other half of all the Co atoms (Co^{3+}) are in their low-spin state. [19, 36] This leads to an interesting magnetic ordering, leaving out all Co^{3+} ions resulting in rather long magnetic exchange paths for the Co^{2+} ions.

The Curie-Weiss temperature θ_{CW} = − 89 K indicates predominant antiferromagnetic exchange interactions at low temperature in $La_2CoO_{4.25}$ and the estimated value of frustration parameter, $f = |\theta_{CW}|/T_N$ = 2.47, suggests that this compound is a moderated frustrated magnetic system.[37]

The deviation of the inverse susceptibility below the θ_{CW} limit approaching T_N could suggest a ferrimagnetic or canted antiferromagnetic transition, which is also consistent with the FC/ZFC divergence below T_N. Low temperature M-H loops measurements are on-going with

the determination of magnetic structure by neutron diffraction, and they will be the object of a future paper.

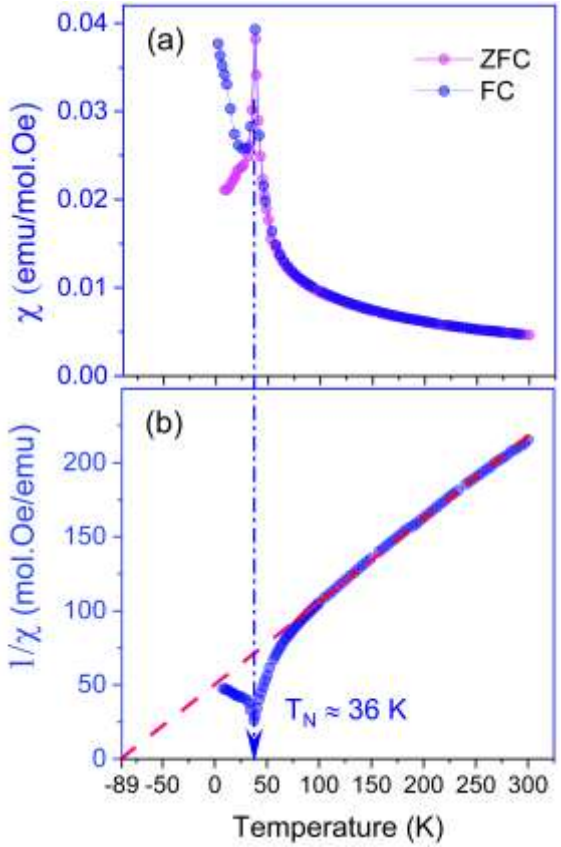

Figure 10. (a) Temperature evolution of the field-cooled (FC) and the zero-field-cooled (ZFC) molar magnetic susceptibility of $La_2CoO_{4.25}$, showing the well-defined inset of antiferromagnetic ordering at $T_N = 36$ K. (b) Inverse susceptibility $1/\chi$ fitted with the modified Curie−Weiss law in the 100-300 K temperature range (red dashed line).

Elastic **Q** scans (where **Q** is the scattering vector) were carried out above and below the antiferromagnetic transition temperature (T_N=36 K) as determined by the SQUID measurements, on the triple axis spectrometer IN12 (ILL, Grenoble). At 10 K the (½, 0, 0) reflection has been identified as a purely magnetic peak, as it completely disappears at 50 K (inset Figure 11a). The temperature dependence of its intensity (Figure 11a) confirms the onset

of the antiferromagnetic order at T_N = 36 K, in a good agreement with the magnetic measurements. It is worth to note that the neutron incident beam had extremely low higher-order harmonic contamination due to the use of a velocity selector as a filter, thus this reflection is surely indicative of a magnetic origin.

To search for additional magnetic peaks, a Q scan performed at 10 K (in red) and 50 K (in blue), along the direction **Q = (H, 1-H, 0)**, with $0 \leq H \leq 1$, as shown in Figure 11b. Together with two structural Bragg's peaks at (010) and (100), a clear magnetic intensity is observed for Q = (½, ½,0) at 10 K, not present at 50 K, i.e. above the T_N. As found in the single crystal X-ray diffraction, the presence of the (010) and (100) reflections, which are not allowed in the *F* unit cell, suggests a *P*-symmetry. The observation of magnetic Bragg peaks at half-L and half-K positions suggests a complex magnetic structure, where the parameters could be obtained either by doubling the *a*, and *b* parameters implying several propagation vectors. The magnetic structure determination is ongoing.

In order to clarify the origin of the satellite peaks observed in the X ray single crystal diffraction patterns, a **Q**-scan has been performed along the direction **Q** = (H, 1.5 - H, 0) at 10 K (Figure 11c), with 0.5≤H≤1, following the arrow in Figure 7b. Besides the (0.5, 1, 0) and (1, 0.5, 0) reflections, which can be indexed by the modulation vector and therefore due to the order of oxygen, the (1.5, 0, 0) does not correspond to this scheme. This supports the hypothesis of the Co^{2+}/Co^{3+} a checkerboard type charge order as discussed above. However, its intensity is quite high suggesting a magnetic contribution.

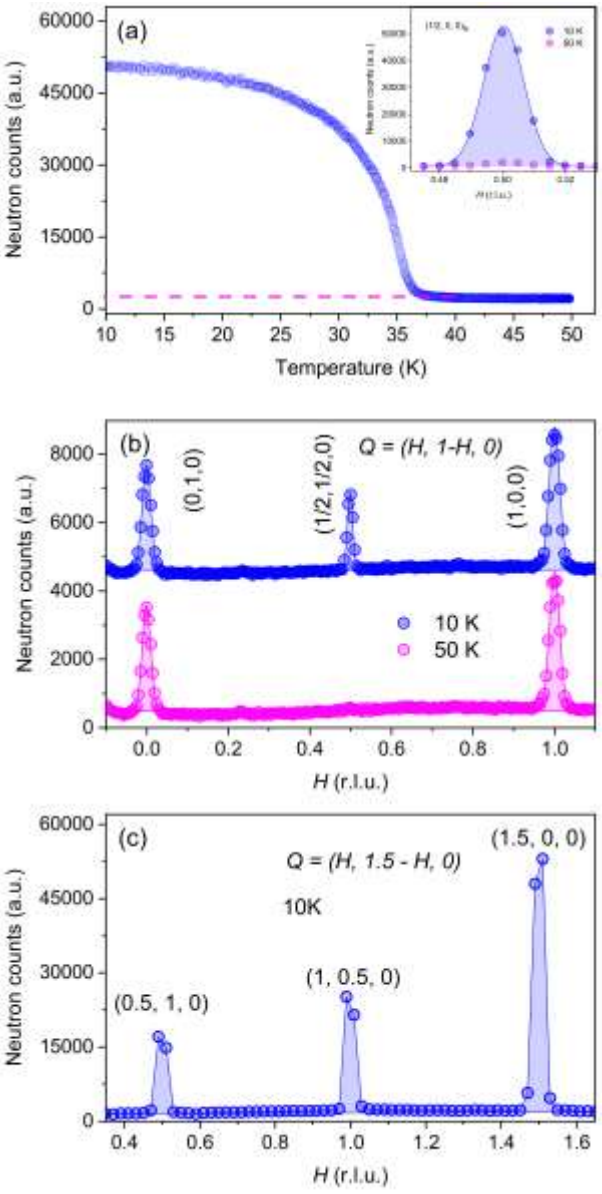

Figure 11. (a) Temperature dependence of the (1/2, 0, 0) magnetic peak (in the inset) intensity showing the antiferromagnetic ordering inset at T_N = 36 K. (b) Elastic neutrons scans in $La_2CoO_{4.25}$ single crystals along the **Q** = (H, 1-H,0) direction performed at 10 K (blue points) and 50 K (red points). For clarity, the blue curve has been shifted. (c) Elastic neutrons scans along the **Q** = (H, 1.5-H,0) direction performed at 10 K, showing the presence of satellite reflections attributable to oxygen order but also to the Co^{2+}/Co^{3+} charge order. The intensity is in number of counts per 20000 monitor counts, corresponding roughly to 3 s/step, for (a-b), and per 50000 monitor counts (7.5 s/step) for (c).

Conclusion

Large and high quality single-crystals of $La_2CoO_{4.25}$ were successfully grown with the help of a mirror furnace, using the floating zone method. The main problem to overcome for crystal growth was related to the LCO incongruent melting and associated difficult nucleation and growth behaviour. Instead of separately preparing a pre-enriched CoO seed rod as it is usually the case, a stable melt zone was obtained here using stoichiometric feed and seed rods. In this case, the molten zone regulates itself with the solidification of La_2O_3, thus continuously enriching the quantity of Co in the traveling solvent. The optimized growth parameters allowed obtaining large and homogeneous crystals without significant mosaic spread and stacking faults, as confirmed by diffraction measurements (X-rays and neutrons) as well as scanning electron microscopy coupled with elemental analysis (EDS). X-ray single crystal diffraction revealed in addition to the main reflections, a huge amount of satellite reflections. Their intensities are nevertheless significant, suggesting strong structural modulations induced by oxygen ordering, as confirmed by neutron diffraction, but also charge ordering of Co^{2+}/Co^{3+}. Magnetic measurements coupled with neutron elastic scattering experiments show the inset of an antiferromagnetic order at about 36 K, with a complex spin structure, which is presently under investigation.

The large size and the excellent quality of the grown crystals make them perfectly suitable for inelastic neutron scattering experiments. Some first spin wave excitations have been unveiled by preliminary but very promising measurements on IN12 which are outside the scope of this paper, and will be further explored.

AUTHOR INFORMATION

Corresponding Author

* monica.ceretti@umontpellier.fr

Funding Sources

Financial support from the French National Research Agency (ANR) through the project "ExODiff" (ANR-19-CE05-0041) is gratefully acknowledged.

ACKNOWLEDGMENT

The authors acknowledge the use of neutron beam time on the diffractometers ORION and HRPT at the Paul Scherrer Institut (CH) as well as on the triple axis IN12 at ILL (CRG instrument operated by FZ Jülich in cooperation with CEA Grenoble). The support from the "Plateforme d'Analyse et de Caractérisation" and the "Plateforme de Microscopie Électronique et Analytique**"** of the ICGM Montpellier are gratefully acknowledged.

REFERENCES

1. Tranquada, J. M.; Lorenzo, J. E.; Buttrey, D. J.; Sachan, V. Cooperative ordering of holes and spins in $La_2NiO_{4.125}$. *Phys. Rev. B* **1995,** 52 (5), 3581-3595.

2. Fujita, M.; Hiraka, H.; Matsuda, M.; Matsuura, M.; M. Tranquada, J.; Wakimoto, S.; Xu, G.; Yamada, K. Progress in Neutron Scattering Studies of Spin Excitations in High-Tc Cuprates. *J. Phys. Soc. Jpn.* **2011,** 81 (1), 011007.

3. Nakajima, K.; Endoh, Y.; Hosoya, S.; Wada, J.; Welz, D.; Mayer, H.-M.; Graf, H.-A.; Steiner, M. Neutron Scattering Study of Oxygen Ordering and Magnetic Correlations in $La_2NiO_{4.11}$ and $La_2NiO_{4.125}$. *J. Phys. Soc. Jpn.* **1997,** 66 (3), 809-817.

4. Rao, C. N. R. Charge, Spin, and Orbital Ordering in the Perovskite Manganates, $Ln_{1-x}A_xMnO_3$ (Ln = Rare Earth, A = Ca or Sr). *J. Phys. Chem. B* **2000,** 104 (25), 5877-5889.

5. Boehm, E.; Bassat, J. M.; Dordor, P.; Mauvy, F.; Grenier, J. C.; Stevens, P. Oxygen diffusion and transport properties in non-stoichiometric $Ln_2NiO_{4+\delta}$ oxides. *Solid State Ionics* **2005,** 176 (37–38), 2717-2725.

6. Chauveau, F.; Mougin, J.; Mauvy, F.; Bassat, J.-M.; Grenier, J.-C. Development and operation of alternative oxygen electrode materials for hydrogen production by high temperature steam electrolysis. *Int. J. Hydrog. Energy* **2011,** 36 (13), 7785-7790.

7. Ferchaud, C.; Grenier, J.-C.; Zhang-Steenwinkel, Y.; van Tuel, M. M. A.; van Berkel, F. P. F.; Bassat, J.-M. High performance praseodymium nickelate oxide cathode for low temperature solid oxide fuel cell. *J. Power Sources* **2011,** 196 (4), 1872-1879.

8. Ceretti, M.; Wahyudi, O.; Cousson, A.; Villesuzanne, A.; Meven, M.; Pedersen, B.; Bassat, J. M.; Paulus, W. Low temperature oxygen diffusion mechanisms in $Nd_2NiO_{4+\delta}$ and $Pr_2NiO4_{+\delta}$ via large anharmonic displacements, explored by single crystal neutron diffraction. *J. Mater. Chem. A* **2015,** 3 (42), 21140-21148.

9. Kushima, A.; Parfitt, D.; Chroneos, A.; Yildiz, B.; Kilner, J. A.; Grimes, R. W. Interstitialcy diffusion of oxygen in tetragonal $La_2CoO_{4+\delta}$. *Phys. Chem. Chem. Phys.* **2011,** 13 (6), 2242-2249.

10. Dutta, R.; Maity, A.; Marsicano, A.; Ceretti, M.; Chernyshov, D.; Bosak, A.; Villesuzanne, A.; Roth, G.; Perversi, G.; Paulus, W. Long-range oxygen ordering linked to

topotactic oxygen release in $Pr_2NiO_{4+\delta}$ fuel cell cathode material. *J. Mater. Chem. A* **2020,** 8 (28), 13987-13995.

11. Girgsdies, F.; Schöllhorn, R. Spontaneous topotactic oxidation of La_2CoO_4 at room temperature. *Solid State Commun.* **1994,** 91 (2), 111-112.

12. Nemudry, A.; Rudolf, P.; Schöllhorn, R. Room temperature topotactic oxidation of lanthanum cobalt oxide $La_2CoO_{4.0}$. *Solid State Ionics* **1998,** 109 (3), 213-222.

13. Le Dréau, L.; Prestipino, C.; Hernandez, O.; Schefer, J.; Vaughan, G.; Paofai, S.; Perez-Mato, J. M.; Hosoya, S.; Paulus, W. Structural Modulation and Phase Transitions in $La_2CoO_{4.14}$ Investigated by Synchrotron X-ray and Neutron Single-Crystal Diffraction. *Inorg. Chem.* **2012,** 51 (18), 9789-9798.

14. Maity, S. R.; Ceretti, M.; Keller, L.; Schefer, J.; Meven, M.; Pomjakushina, E.; Paulus, W. Interdependent scaling of long-range oxygen and magnetic ordering in nonstoichiometric $Nd_2NiO_{4.10}$. *Phys. Rev. Mater.* **2021,** 5 (1), 014401.

15. Drees, Y.; Li, Z. W.; Ricci, A.; Rotter, M.; Schmidt, W.; Lamago, D.; Sobolev, O.; Rütt, U.; Gutowski, O.; Sprung, M.; Piovano, A.; Castellan, J. P.; Komarek, A. C. Hour-glass magnetic excitations induced by nanoscopic phase separation in cobalt oxides. *Nat. Commun.* **2014,** 5 (1), 5731.

16. Guo, H.; Schmidt, W.; Tjeng, L. H.; Komarek, A. C. Charge correlations in cobaltates $La_{2-x}Sr_x$ CoO_4. *Phys. Status Solidi - Rapid Res. Lett.* **2015,** 9 (10), 580-582.

17. Li, Z. W.; Drees, Y.; Kuo, C. Y.; Guo, H.; Ricci, A.; Lamago, D.; Sobolev, O.; Rütt, U.; Gutowski, O.; Pi, T. W.; Piovano, A.; Schmidt, W.; Mogare, K.; Hu, Z.; Tjeng, L. H.; Komarek, A. C. Incommensurate spin correlations in highly oxidized cobaltates $La_{2-x}Sr_xCoO4$. *Sci. Rep.* **2016,** 6 (1), 25117.

18. Babkevich, P.; Freeman, P. G.; Enderle, M.; Prabhakaran, D.; Boothroyd, A. T. Direct evidence for charge stripes in a layered cobalt oxide. *Nat. Commun.* **2016,** 7 (1), 11632.

19. Helme, L. M.; Boothroyd, A. T.; Coldea, R.; Prabhakaran, D.; Frost, C. D.; Keen, D. A.; Regnault, L. P.; Freeman, P. G.; Enderle, M.; Kulda, J. Magnetic order and dynamics of the charge-ordered antiferromagnet $La_{1.5}Sr0_{.5}CoO_4$. *Phys. Rev. B* **2009,** 80 (13), 134414.

20. Dong, S. T.; Sun, N.; Zhang, B. B.; Zhang, F.; Yao, S. H.; Zhou, J.; Zhang, S. T.; Gu, Z. B.; Chen, Y. B.; Chen, Y. F. Crystal growth, structure, and dielectric properties of layered cobaltates $La_{2-x}Sr_xCoO_4$ (x=0.4, 0.5, and 0.6) single crystal. *Materials Research Bulletin* **2015,** 61, 352-356.

21. Ghorbani-Moghadam, T.; Kompany, A.; Bagheri-Mohagheghi, M. M.; Abrishami, M. E. Cobalt spin states investigation of Ruddlesden-Popper $La_{2-x}Sr_xCoO_4$, using X-ray diffraction and infrared spectroscopy. *J. Magn. Magn. Mater.* **2018,** 465, 768-774.

22. Maity, A.; Dutta, R.; Marsicano, A.; Piovano, A.; Stewart, J. R.; Paulus, W. Magnetic excitations in long-range stripe-ordered $Pr_2NiO_{4+\delta}$. *Phys. Rev. B* **2021,** 103 (10), L100401.

23. Yamada, K.; Matsuda, M.; Endoh, Y.; Keimer, B.; Birgeneau, R. J.; Onodera, S.; Mizusaki, J.; Matsuura, T.; Shirane, G. Successive antiferromagnetic phase transitions in single-crystal La_2CoO_4. *Phys. Rev. B* **1989,** 39 (4), 2336-2343.

24. Babkevich, P.; Prabhakaran, D.; Frost, C. D.; Boothroyd, A. T. Magnetic spectrum of the two-dimensional antiferromagnet La_2CoO_4 studied by inelastic neutron scattering. *Phys. Rev. B* **2010,** 82 (18), 184425.

25. Le Toquin, R.; Paulus, W.; Cousson, A.; Dhalenne, G.; Revcolevschi, A. Interstitial and apical oxygen order–disorder in $La_2CoO_{4+\delta}$ observed by single-crystal neutron and X-ray diffraction. *Physica B: Condensed Matter* **2004,** 350 (1, Supplement), E269-E272.

26. Kajitani, T.; Hosoya, S.; Hiraga, K.; Fukuda, T. Tetragonal-Orthorhombic Phase Transition of La_2CoO_{4-x}. *J. Phys. Soc. Jpn.* **1990,** 59 (2), 562-570.

27. Rodríguez-Carvajal, J. Recent developments of the program FullProf. Commission for Powder Diffraction. *IUCr Newsletter* **2001,** 26, 12-19. The complete FULLPROF suite can be obtained from: http://www.ill.eu/sites/fullprof/index.html.

28. Momma, K.; Izumi, F. VESTA 3 for three-dimensional visualization of crystal, volumetric and morphology data. *J. Appl. Crystallogr.* **2011,** 44 (6), 1272-1276.

29. ORION: Test Diffractometer. https://www.psi.ch/fr/sinq/orion

30. Zhang, W.-W.; Povoden-Karadeniz, E.; Xu, H.; Chen, M. Thermodynamic Modeling of the La-Co-O System. *J. Phase Equilib. Diffus.* **2019,** 40 (2), 219-234.

31. Ceretti, M.; Wahyudi, O.; André, G.; Meven, M.; Villesuzanne, A.; Paulus, W. $(Nd/Pr)_2NiO_{4+\delta}$: Reaction Intermediates and Redox Behavior Explored by in Situ Neutron Powder Diffraction during Electrochemical Oxygen Intercalation. *Inorg. Chem.* **2018,** 57 (8), 4657-4666.

32. Wahyudi, O.; Ceretti, M.; Weill, I.; Cousson, A.; Weill, F.; Meven, M.; Guerre, M.; Villesuzanne, A.; Bassat, J. M.; Paulus, W. Growth of high quality single crystals of strontium doped (Nd,Pr)-nickelates, $Nd_{2-x}Sr_xNiO_{4+\delta}$ and $Pr_{2-x}Sr_xNiO_{4+\delta}$. *CrystEngComm* **2015,** 17 (33), 6278-6285.

33. Paulus, W.; Cousson, A.; Dhalenne, G.; Berthon, J.; Revcolevschi, A.; Hosoya, S.; Treutmann, W.; Heger, G.; Le Toquin, R. Neutron diffraction studies of stoichiometric and oxygen intercalated La_2NiO_4 single crystals. *Solid State Sciences* **2002,** 4 (5), 565-573.

34. Maity, A.; Dutta, R.; Sendtskyi, O.; Ceretti, M.; Lebranchu, A.; Chernyshov, D.; Bosak, A.; Paulus, W. Exploring Fast Room Temperature Oxygen Diffusion in $Pr_2NiO_{4+\delta}$ Stand-Alone Single-Crystalline Electrodes. *Chem. Mater.* **2022,** 34 (1), 414-421.

35. Moritomo, Y.; Higashi, K.; Matsuda, K.; Nakamura, A. Spin-state transition in layered perovskite cobalt oxides: $La_{2-x}Sr_xCoO_4$ ($0.4 \leqslant x \leqslant 1.0$)). *Phys. Rev. B* **1997,** 55 (22), R14725-R14728.

36. Hollmann, N.; Haverkort, M. W.; Cwik, M.; Benomar, M.; Reuther, M.; Tanaka, A.; Lorenz, T. Anisotropic susceptibility of $La_{2-x}Sr_xCoO_4$ related to the spin states of cobalt. *New J. Phys.* **2008,** 10 (2), 023018.

37. Ramirez, A. P. Geometrical frustration in magnetism. *Czech. J. Phys.* **1996,** 46 (6), 3247.

For Table of Contents Use Only

Growth and oxygen stoichiometry control of high quality $La_2CoO_{4+\delta}$ single crystals ($\delta = 0.25$)

Ruben De Barros, Monica Ceretti, Wolfgang Schmidt, Vladimir Y. Pomjakushin, Werner Paulus

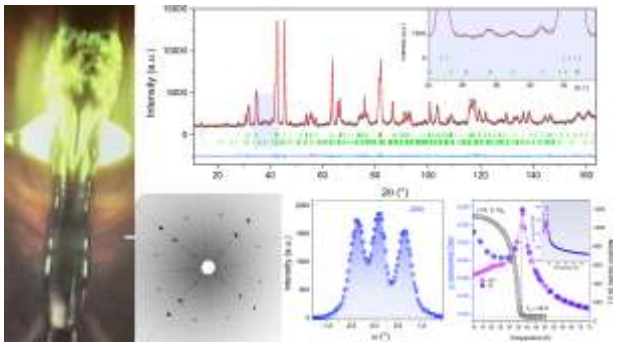

SYNOPSIS. Centimeter sized $La_2CoO_{4.25}$ single crystals were grown by travelling solvent zone in a mirror furnace. Further characterizations by X-ray and neutron diffraction highlight their good quality as well as a complex structure with a 2D modulation vector related to oxygen ordering.